Amplitude and polarization modulated hyperspectral Stimulated Raman Scattering Microscopy

Andreana, Marco; Houle, Marie-Andrée; Moffatt, Douglas J.; Ridsdale, Andrew; Buettner, Edlef; Légaré, François; Stolow, Albert

Publisher's version / Version de l'éditeur:
https://doi.org/10.1364/OE.23.028119
Optics Express, 23, 22, pp. 28119-28131, 2015-10-19

Amplitude and polarization modulated hyperspectral Stimulated Raman Scattering Microscopy

Marco Andreana,[1,2,6] **Marie-Andrée Houle,**[1,3,6] **Douglas J. Moffatt,**[1] **Andrew Ridsdale,**[1] **Edlef Buettner,**[4] **François Légaré**[3] **and Albert Stolow**[1,2,5,*]

[1] *QPSS Program, Security and Disruptive Technologies, National Research Council, Ottawa, ON, K1A 0R6, Canada*

[2]*Department of Physics, University of Ottawa, Ottawa, ON, K1N 6N5, Canada*

[3]*INRS-ÉMT, Varennes, QC, J3X 1S2, Canada*

[4]*APE Angewandte Physik und Elektronik GmbH Plauener Str. 163-165, Haus N13053 Berlin, Germany*

[5]*Department of Chemistry, University of Ottawa, Ottawa, ON, K1N 6N5, Canada*

[6]*These authors contributed equally to this work.*

[*]*Albert.Stolow@nrc.ca*

Abstract: We present a simple hyperspectral Stimulated Raman Scattering (SRS) microscopy method based on spectral focusing of chirped femtosecond pulses, combined with amplitude (AM) and polarization (PM) modulation. This approach permits the imaging of low concentration components with reduced background signals, combined with good hyperspectral resolution and rapid spectral scanning. We demonstrate, using PM-SRS in a Raman loss configuration, the spectrally resolved detection of deuterated dimethyl sulfoxide (DMSO-d6) at concentrations as low as 0.039 % (5.5 *mM*). In general, background signals due to cross-phase modulation (XPM), two-photon absorption (TPA) and thermal lensing (TL) can reduce the contrast in SRS microscopy. We show that the nonresonant background signal contributing to the SRS signal is, in our case, largely due to XPM. Polarization modulation of the Stokes beam eliminates the nonresonant XPM background, yielding high quality hyperspectral scans at low analyte concentration. The flexibility of our combined AM-PM approach, together with the use of variable modulation frequency and lock-in phase, should allow for optimization of SRS imaging in more complex samples.

OCIS codes: (180.4315) Nonlinear microscopy; (290.5910) Scattering, stimulated Raman; (300.6450) Spectroscopy, Raman.

References and links

1. A. Zumbusch, G. Holtom, and X. Xie, "Three-dimensional vibrational imaging by coherent anti-stokes Raman scattering," Phys. Rev. Lett. **82**, 4142–4145 (1999).
2. E. O. Potma and X. S. Xie, "CARS microscopy for biology and medicine," Opt. Photonics News **15**, 40 (2004).
3. C. L. Evans and X. S. Xie, "Coherent anti-stokes Raman scattering microscopy: Chemical imaging for biology and medicine," Annu. Rev. Anal. Chem. **1**, 883–909 (2008).
4. J.-X. Cheng, A. Volkmer, L. D. Book, and X. S. Xie, "An epi-detected coherent anti-stokes Raman scattering (e-CARS) microscope with high spectral resolution and high sensitivity," J. Phys. Chem. B **105**, 1277–1280 (2001).

#243330 Received 22 Jun 2015; revised 8 Sep 2015; accepted 11 Oct 2015; published 19 Oct 2015

5. C. H. Camp Jr and M. T. Cicerone, "Chemically sensitive bioimaging with coherent Raman scattering," Nat. Photonics **9**, 295–305 (2015).
6. A. F. Pegoraro, A. D. Slepkov, A. Ridsdale, D. J. Moffatt, and A. Stolow, "Hyperspectral multimodal CARS microscopy in the fingerprint region," J. Biophotonics **7**, 49–58 (2014).
7. T. Hellerer, A. M. Enejder, and A. Zumbusch, "Spectral focusing: High spectral resolution spectroscopy with broad-bandwidth laser pulses," Appl. Phys. Lett. **85**, 25 (2004).
8. I. Rocha-Mendoza, W. Langbein, and P. Borri, "Coherent anti-stokes Raman microspectroscopy using spectral focusing with glass dispersion," Appl. Phys. Lett. **93**, 201103 (2008).
9. A. F. Pegoraro, A. Ridsdale, D. J. Moffatt, Y. Jia, J. P. Pezacki, and A. Stolow, "Optimally chirped multimodal CARS microscopy based on a single Ti:sapphire oscillator," Opt. Express **17**, 2984 (2009).
10. W. Langbein, I. Rocha-Mendoza, and P. Borri, "Single source coherent anti-stokes Raman microspectroscopy using spectral focusing," Appl. Phys. Lett. **95**, 081109 (2009).
11. A. D. Slepkov, A. Ridsdale, A. F. Pegoraro, D. J. Moffatt, and A. Stolow, "Multimodal CARS microscopy of structured carbohydrate biopolymers," Biomed. Opt. Express **1**, 1347 (2010).
12. B.-C. Chen, J. Sung, and S.-H. Lim, "Chemical imaging with frequency modulation coherent anti-stokes Raman scattering microscopy at the vibrational fingerprint region," J. Phys. Chem. B **114**, 16871–16880 (2010).
13. B.-C. Chen, J. Sung, X. Wu, and S.-H. Lim, "Chemical imaging and microspectroscopy with spectral focusing coherent anti-stokes Raman scattering," J. Biomed. Opt. **16**, 021112 (2011).
14. R. J. H. Clark and R. E. Hester, *Advances in Non-Linear Spectroscopy (Advances in Spectroscopy)* (Wiley, 1988).
15. E. O. Potma, C. L. Evans, and X. S. Xie, "Heterodyne coherent anti-stokes Raman scattering (CARS) imaging," Opt. Lett. **31**, 241 (2006).
16. H. A. Rinia, M. Bonn, and M. Muller, "Quantitative multiplex CARS spectroscopy in congested spectral regions," J. Phys. Chem. B **110**, 4472–4479 (2006).
17. A. M. Barlow, K. Popov, M. Andreana, D. J. Moffatt, A. Ridsdale, A. D. Slepkov, J. L. Harden, L. Ramunno, and A. Stolow, "Spatial-spectral coupling in coherent anti-stokes Raman scattering microscopy," Opt. Express **21**, 15298 (2013).
18. K. I. Popov, A. F. Pegoraro, A. Stolow, and L. Ramunno, "Image formation in CARS and SRS: effect of an inhomogeneous nonresonant background medium," Opt. Lett. **37**, 473–475 (2012).
19. K. I. Popov, A. F. Pegoraro, A. Stolow, and L. Ramunno, "Image formation in CARS microscopy: effect of the Gouy phase shift," Opt. Express **19**, 5902 (2011).
20. F. Ganikhanov, C. L. Evans, B. G. Saar, and X. S. Xie, "High-sensitivity vibrational imaging with frequency modulation coherent anti-stokes Raman scattering (FM CARS) microscopy," Opt. Lett. **31**, 1872 (2006).
21. Y. Liu, Y. J. Lee, and M. T. Cicerone, "Broadband CARS spectral phase retrieval using a time-domain Kramers–Kronig transform," Opt. Lett. **34**, 1363–1365 (2009).
22. E. Ploetz, S. Laimgruber, S. Berner, W. Zinth, and P. Gilch, "Femtosecond stimulated Raman microscopy," Appl. Phys. B **87**, 389–393 (2007).
23. C. W. Freudiger, W. Min, B. G. Saar, S. Lu, G. R. Holtom, C. He, J. C. Tsai, J. X. Kang, and X. S. Xie, "Label-free biomedical imaging with high sensitivity by stimulated Raman scattering microscopy," Science **322**, 1857–1861 (2008).
24. P. Nandakumar, A. Kovalev, and A. Volkmer, "Vibrational imaging based on stimulated Raman scattering microscopy," New J. Phys. **11**, 033026 (2009).
25. Y. Ozeki, F. Dake, S. Kajiyama, K. Fukui, and K. Itoh, "Analysis and experimental assessment of the sensitivity of stimulated Raman scattering microscopy," Opt. Express **17**, 3651 (2009).
26. D. Zhang, M. N. Slipchenko, and J.-X. Cheng, "Highly sensitive vibrational imaging by femtosecond pulse stimulated Raman loss," J. Phys. Chem. Lett. **2**, 1248–1253 (2011).
27. D. Fu, T. Ye, T. E. Matthews, B. J. Chen, G. Yurtserver, and W. S. Warren, "High-resolution in vivo imaging of blood vessels without labeling," Opt. Lett. **32**, 2641 (2007).
28. P. Berto, E. R. Andresen, and H. Rigneault, "Background-free stimulated Raman spectroscopy and microscopy," Phys. Rev. Lett. **112**, 053905 (2014).
29. K. Ekvall, P. van der Meulen, C. Dhollande, L.-E. Berg, S. Pommeret, R. Naskrecki, and J.-C. Mialocq, "Cross phase modulation artifact in liquid phase transient absorption spectroscopy," J. Appl. Phys. **87**, 2340 (2000).
30. K. Uchiyama, A. Hibara, H. Kimura, T. Sawada, and T. Kitamori, "Thermal lens microscope," Jpn. J. Appl. Phys. **39**, 5316–5322 (2000).
31. S. Berciaud, L. Cognet, G. Blab, and B. Lounis, "Photothermal heterodyne imaging of individual nonfluorescent nanoclusters and nanocrystals," Phys. Rev. Lett. **93**, 257402 (2004).
32. S. Hiki, K. Mawatari, A. Hibara, M. Tokeshi, and T. Kitamori, "UV excitation thermal lens microscope for sensitive and nonlabeled detection of nonfluorescent molecules," Anal. Chem. **78**, 2859–2863 (2006).
33. C. W. Freudiger, W. Min, G. R. Holtom, B. Xu, M. Dantus, and X. Sunney Xie, "Highly specific label-free molecular imaging with spectrally tailored excitation-stimulated Raman scattering (STE-SRS) microscopy," Nat. Photonics **5**, 103–109 (2011).
34. C. W. Freudiger, M. B. J. Roeffaers, X. Zhang, B. G. Saar, W. Min, and X. S. Xie, "Optical Heterodyne-Detected Raman-Induced Kerr Effect (OHD-RIKE) Microscopy," J. Phys. Chem. B **115**, 5574–5581 (2011).

#243330 Received 22 Jun 2015; revised 8 Sep 2015; accepted 11 Oct 2015; published 19 Oct 2015

35. F. Munhoz, S. Brustlein, R. Hostein, P. Berto, S. Brasselet, and H. Rigneault, "Polarization resolved stimulated raman scattering: probing depolarization ratios of liquids," J. Raman Spectrosc. **43**, 419–424 (2012).
36. W. N. Martens, R. L. Frost, J. Kristof, and J. Theo Kloprogge, "Raman spectroscopy of dimethyl sulphoxide and deuterated dimethyl sulphoxide at 298 and 77 K," J. Raman Spectrosc. **33**, 84–91 (2002).
37. P. N. Butcher and D. Cotter, *The Elements of Nonlinear Optics* (Cambridge University, 1990).
38. R. W. Boyd, *Nonlinear Optics* (Academic, 2008), 3rd ed.
39. M. D. Levenson, *Introduction to Nonlinear Laser Spectroscopy* (Academic, 1982).
40. A. De Santis, R. Frattini, M. Sampoli, V. Mazzacurati, M. Nardone, M. Ricci, and G. Ruocco, "Raman spectra of water in the translational and librational regions: I. study of the depolarization ratio," Mol. Phys. **61**, 1199–1212 (1987).
41. B. Schrader and W. Meier, *Raman/IR Atlas of Organic Compounds* (Verlag Chemie GmbH, 1976).
42. J. Moger, N. L. Garrett, D. Begley, L. Mihoreanu, A. Lalatsa, M. V. Lozano, M. Mazza, A. Schatzlein, and I. Uchegbu, "Imaging cortical vasculature with stimulated Raman scattering and two-photon photothermal lensing microscopy," J. Raman Spectrosc. **43**, 668–674 (2012).

1. Introduction

Coherent Raman scattering (CRS) is a molecule-specific third-order nonlinear optical imaging method wherein contrast is achieved via vibrational Raman resonances [1–5]. This technique is based on the interaction of laser beams at pump frequency ω_p and Stokes frequency ω_S with their frequency difference $\Delta\omega = \omega_p - \omega_S$ matching the resonant frequency Ω of a specific molecular vibrational transition of a target molecule within the sample. Amongst the different CRS techniques, the most widely used is coherent anti-Stokes Raman scattering (CARS) in which the detected signal is the generated blue-shifted anti-Stokes ($\omega_{AS} = 2\omega_p - \omega_S$) beam, as illustrated in Fig. 1(a). The prime utility of this method is based on the generated anti-Stokes beam being in some cases enhanced by orders of magnitude as compared to spontaneous Raman scattering. This is because CARS is a stimulated rather than spontaneous process and the magnitude of the CARS signal (I_{CARS}) is proportional to the square of the pump intensity (I_p) and is linear with the Stokes intensity (I_S). Spectral-focusing-based CARS microscopy [6,7] is a particularly simple and flexible implementation which permits rapid hyperspectral imaging around a specific Raman shift, recording a partial Raman spectrum or combining CARS with other techniques in order to achieve multimodal imaging. Spectral focusing allows for both rapid contrast-based imaging and for the fastest spectral scanning, over a set range (e.g. $<$ 1000 cm^{-1}), of the Raman spectrum [5]. Such hyperspectral imaging has been widely used to study live cells and tissues [7–13]. Here we demonstrate, as a proof-of-concept, a new combined amplitude (AM) and polarization (PM) modulation scheme for optimizing spectral focusing Stimulated Raman Scattering (SRS) microscopy. In samples where cross-phase modulation (XPM) dominates the background, we show that PM largely eliminates this effect, leading to rapid hyperspectral imaging at low analyte concentrations.

The analysis of CARS signal intensity and spectral lineshape is complicated by the coherent addition of the resonant signal with a non-resonant background (NRB) signal due to electronic four wave mixing (FWM) within the sample [14]. The NRB signal can overwhelm the resonant signal in cases where the concentration of Raman resonant molecules is low [15]. This causes spectral distortions in the Raman spectrum [16], coherent imaging artifacts [17–19] and reduces the chemical detection sensitivity [20]. Quantitative measurements are complicated by all these unwanted effects, as well as by the nonlinear dependence of the CARS signal on the concentration of target molecules. The careful use of phase retrieval methods, such as the time-domain Kramers-Kronig transform [21], removes the NRB contribution, yielding high quality Raman-like spectra at low analyte concentrations. Nevertheless, phase retrieval does not eliminate spatial-spectral coupling in CARS imaging [17] which can become an important distortion effect at low analytes concentrations. We note that SRS is unaffected by spatial-spectral coupling.

#243330 Received 22 Jun 2015; revised 8 Sep 2015; accepted 11 Oct 2015; published 19 Oct 2015

SRS has gained popularity more recently because it addresses many of these concerns [17, 22–26]. The SRS signal is generated at the frequency of an incident beam which acts as a local oscillator. Indeed, SRS is based on the energy transfer between the pump and the Stokes beams (Fig. 1(a)) where the measured signal may either be a power gain in the Stokes beam (Stimulated Raman Gain - SRG) or a loss in the pump beam (Stimulated Raman Loss - SRL). The SRL process is illustrated in Fig. 1(c). The SRS signal provides spectral information similar to spontaneous Raman and is linearly proportional to the target molecule concentration. Despite being free from the four-wave mixing (NRB) processes which plague CARS microscopy, SRS is not "background free". Indeed, SRS contains parasitic background signals which may be spectrally overlapped with the SRS signal. These unwanted signals can be classified as being due to two general categories of nonlinear effects: two photon absorption (TPA) and nonlinear transient scattering. TPA can arise from the simultaneous absorption of one pump and one Stokes, of two pump or of two Stokes photons. The former is seen as a loss by the detection system and therefore is detected as a SRL signal [27, 28]. In contrast, nonlinear transient scattering arises from the refractive index changes induced by the pump beam and experienced by the Stokes beam. It is caused by two effects: (i) the purely nonresonant and instantaneous cross phase modulation (XPM) [29], and (ii) thermal lensing (TL) or thermal scattering, a time-averaged multiple pulse response which results from temperature-induced variations of the refractive index due to absorption of either the pump or Stokes beams [28, 30]. TPA can be reduced by using longer wavelengths for both the pump and the Stokes [26] whereas nonlinear transient scattering effects can be reduced by using collection optics with large numerical aperture [23, 26, 31, 32]. Nevertheless, in the case of very weak SRS signals, there remains a need for improved contrast and sensitivity.

In this work, we present a scheme based on AM and PM of one of the two incident beams (see Fig. 1(d)), permitting multimodal imaging with spectral focusing in a hyperspectral implementation, similar to a previously presented hyperspectral CARS arrangement [6]. In contexts different from that presented here, the use of polarization schemes in SRS microscopy was demonstrated previously. For example, polarization modulation at specific frequencies [33] was used to achieve spectral modulation of the pump beam before the microscope but the polarization state at the sample was not modulated. In another example, an AM scheme with variable but unmodulated polarization angle between the pump and the Stokes beams was used for Raman-induced Kerr effect (RIKE) microscopy [34]. Variable but unmodulated polarization was also used the measure the angle-resolved SRS response and the depolarization ratios in specific systems [35]. We note, however, that in these prior schemes, neither the pump nor the Stokes beams were modulated in polarization at the sample, the requirement for the method presented here. For samples in which it is significant, XPM will contribute both when the polarization of the pump and the Stokes beams are parallel and when they are perpendicular. On the other hand, for those Raman bands which are highly polarized, the SRS signal will be maximum when the polarizations are parallel, with almost no SRS signal being produced for perpendicular polarizations. Therefore, modulating the relative pump-Stokes polarization at the sample would successfully minimize the XPM background without adversely affecting the resonant Raman signal. Since TL in unstructured media is relatively insensitive to the incident polarization, this same scheme may also serve to reduce TL-induced background effects. In general, the angular dependence of the SRS response will depend on the symmetry of the Raman mode being probed: in other words, the depolarization ratio is mode specific [35]. This means that a PM-SRS scheme such as presented here will have a spectral contrast which depends on the symmetry of the Raman mode under study. Furthermore, any residual birefringence in the sample may also reduce contrast. These effects are discussed in a following section. Finally, although we present here both CARS and SRS spectra, we emphasize that our goal is not to compare sen-

#243330 Received 22 Jun 2015; revised 8 Sep 2015; accepted 11 Oct 2015; published 19 Oct 2015

sitivity limits between these two modalities. In fact, it is expected that phase-retrieved CARS spectra will have sensitivity limits similar to SRS [5, 25]. Our aim here is to demonstrate that enhanced XPM background suppression can be achieved by PM in spectral focusing SRS microscopy. The paper is organized as follows. In Section 2, we describe the experimental setup and the basic concept of the SRS AM-PM scheme. In Section 3, we present the experimental results and determine the origin of the background signal in the studied samples. We present our conclusions and outlook in Section 4.

2. Experimental setup

The experiments were performed using the chirped pulse (spectral focusing) arrangement shown in Fig. 1(b). This arrangement may be used for either Stimulated Raman Gain (SRG) in the Stokes beam or Stimulated Raman Loss (SRL) in the pump beam. In this manuscript, for technical reasons, we present only the SRL case. We note, however, that the SRG scheme has some advantages when TPA contributes significantly to the background. A Titanium:Sapphire laser (Chameleon, Coherent, USA) produced the Stokes beam with a pulse duration of approximately 200 fs (chirped to $\sim$1.3 ps), centered at a wavelength of 800 nm. The pump beam was generated by a synchronously-pumped OPO (OPO PP auto FAN, APE, Germany), centered at a wavelength of 680 nm with an approximately 200 fs pulse duration (chirped to a pulse length of $\sim$2.5 ps). Due to specific anti-reflections coatings on our existing modulator, we have chosen to demonstrate here SRL, as shown in Fig. 1(c). The experimental setup permits both amplitude modulation (AM) and polarization modulation (PM) hyperspectral coherent Raman microscopy. A Pockels cell (350-160, Conoptics, USA) induced polarization modulation (typically, 1-5 MHz) of the 800 nm Stokes beam. The two polarizations were separated by a polarizing beamsplitter which led to two beams, one shifted by half a modulation period (*beam 2*) as compared to the other (*beam 1*). The polarization angle of *beam 2* was then finely tuned to 90 degrees using a half wave plate (WPH05M-808, Thorlabs, USA) such that its polarization was perpendicular to both *beam 1* and the pump beam. The two 800 nm Stokes beams were then combined using a beam splitter, creating a train of pulses whose relative polarization angle was periodically modulated to be parallel or perpendicular to the pump beam polarization (Fig. 1(d)). Implementing the amplitude modulation (AM) scheme required simply blocking *beam 2*, thereby leaving *beam 1* as the (AM) Stokes beam. The pump and the Stokes beams were combined using a dichroic mirror. A fixed optical path length of glass (25 and 30 cm of SF11 glass for the Stokes and pump beams, respectively) was placed in the paths of the beams so as to induce a positive chirp, allowing for fast tuning of the Raman frequency by time-scanned spectral focusing [6]. The chirped pulse duration of the pump and Stokes beams were, respectively, around 2.5 and 1.3 picoseconds. The time delays between the pump and the Stokes beam were controlled by two translation stages in the Stokes beam path.

The pump and Stokes beam were sent into an inverted microscope (IX-71, Olympus, Japan) and focused into the sample with a microscope objective (UPlanSapo, 20x, NA 0.75, Olympus, Japan). Galvanometer mirrors at the entrance of the microscope allowed the beams to raster scan the sample, providing an image. The pump beam was collected in the forward direction by a microscope objective (LUMPlanFI/IR, 40x, NA 0.8w, Olympus, Japan) and sent into a photodiode (FDS10X10, Thorlabs, USA) after being filtered by two different optical filters (BrightLine 750/SP, Semrock, USA and HQ680/60, Chroma, USA). In the backward direction, a dichroic mirror (Z660DCXR, Chroma, USA) sent the back-reflected CARS signal through a bandpass filter (D605/55M, Chroma, USA) to a photomultiplier tube. A function generator (DS345, Stanford Research Systems, USA) produced the modulation signal for the Pockels cell. We used a square wave modulation at a frequency of 2 MHz, chosen to reduce the contributions of laser noise. The reference signal was also sent into a lock-in amplifier (UHFLI,

#243330 Received 22 Jun 2015; revised 8 Sep 2015; accepted 11 Oct 2015; published 19 Oct 2015

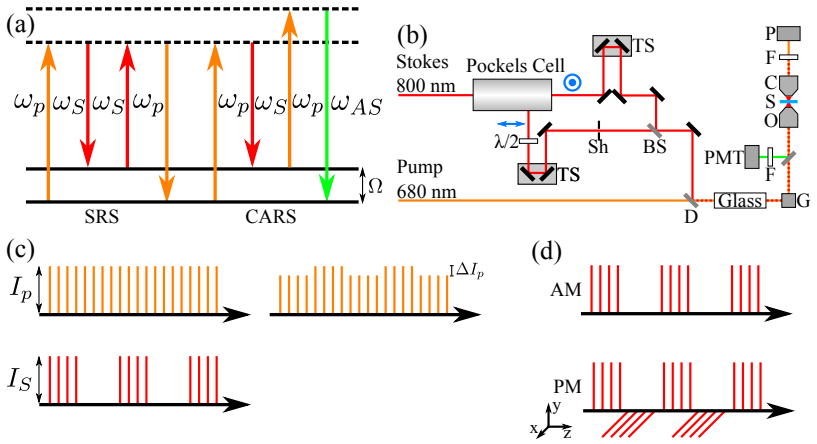

Fig. 1. Principle of AM-PM SRS microscopy. (a) Energy level diagram for SRS and CARS microscopy. (b) Experimental setup for AM-SRS and PM-SRS: (BS) beam splitter, (D) dichroic mirror, (G) galvanometers mirrors, (S) sample, (O) microscope objective, (C) condenser, (P) photodiode, (F) filters, (PMT) photomultiplier tube, (Sh) shutter and ($\lambda/2$) half-wave plate. (c) Stimulated Raman Loss (SRL) scheme used in the present experiment. The analogous Stimulated Raman Gain (SRG) scheme may be readily implemented by applying the AM or PM modulation to the pump beam. (d) A depiction of the AM and PM SRS microscopy scheme. In AM-SRS, the intensity of the Stokes beam is modulated while in PM-SRS, the state of the linear polarization is modulated. A key aspect of the PM scheme is that the total power (Pump+Stokes) transmitted through the sample may be chosen to be invariant, minimizing thermal lensing effects. Importantly, PM-SRS can specifically reduce the XPM background contribution to the signal.

Zurich Instruments) as the reference frequency. The photodiode signal was amplified by a transimpedance amplifier (DHPCA-100, Femto Messtechnik GmbH, Germany) which provided the input to the lock-in amplifier. The lock-in amplifier then extracted the SRS signal at the function generator frequency. A time constant of 20 μs was used and the phase of the lock-in amplifier was adjusted to maximize the SRS signal.

The spectral scans shown were obtained by acquiring images while continuously scanning the time delay between the pump and the Stokes pulses. One data point in the spectrum corresponds to the average intensity across the region of interest (ROI) in an image. By adjusting the chirp parameter of the pump and Stokes beams and the speed of the translation stage, the effective spectral resolution can be varied. In the present case, the scan speed corresponded to 2.3 cm^{-1} per acquisition spectral data point. With the chirp parameters implemented, the Raman spectral resolution was approximately 25 cm^{-1}. Each image (256 $\times$ 256 pixels) took $\sim$2 seconds to acquire and the total acquisition time for a hyperspectral scan was 9 min 20 seconds. The images displayed here have an image pixel size of 1.05 μm and are an average of 5 images with an acquisition time of $\sim$2 seconds per image.

3. Discussion

In order to demonstrate a proof-of-concept for AM-PM-SRS microscopy, with particular interest in hyperspectral imaging at low concentration, we chose to image simple solutions of liquid water and deuterated dimethyl sulfoxide (DMSO-d6) at a range of concentrations. We choose this specific compound because it has an isolated and unambiguous Raman signature in the range 1750 to 2400 cm^{-1}. DMSO-d6 has two Raman resonances at $\sim$ 2125 cm^{-1} and

#243330 Received 22 Jun 2015; revised 8 Sep 2015; accepted 11 Oct 2015; published 19 Oct 2015

$\sim 2000\ cm^{-1}$ [36]. Although we focus here on background mitigation in SRS microscopy, we find it illustrative to compare the more familiar (raw) CARS spectra with SRS spectra of the same sample using the same laser pulses. To that end, in Fig. 2 we presents simultaneously recorded vibrational Raman spectra using AM-SRS and CARS in the spectral region ranging from 1750 to 2400 cm^{-1} at two concentrations. At 10 % (1.4 M) DMSO-d6, the AM-SRS Raman spectrum (Fig. 2(a)) reveals two well separated resonances. In contrast, the raw CARS spectrum (Fig 2(b)) contains a large NRB signal due to electronic FWM: the Raman resonance at $\sim 2150\ cm^{-1}$ is barely visible. At an order of magnitude lower concentration (1.25 % or 0.18 M), shown in the bottom row, the signal becomes considerably smaller. The raw CARS spectrum (Fig. 2(d)) is dominated by the background signal. As is amply discussed elsewhere, the resonant Raman signal can still be extracted from such data using phase retrieval techniques [21]. Importantly, the AM-SRS spectrum still exhibits two clear Raman resonances peaks due to DMSO-d6. However, the AM-SRS spectrum (Fig. 2(c)) now seems to contain a background signal as well.

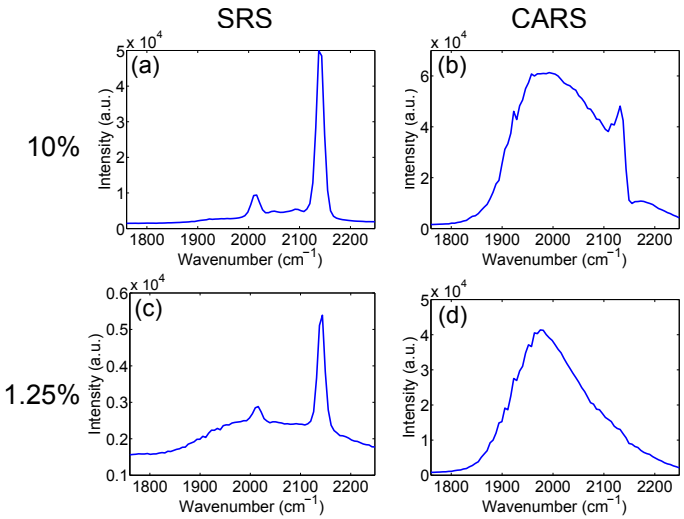

Fig. 2. (a) Amplitude-modulated SRS (AM-SRS) microscopy spectrum and (b) raw CARS spectrum at a concentration of 10 % (1.4 M) DMSO-d6 in water. (c) AM-SRS and (d) raw CARS spectrum at 1.25 % (0.18 M) DMSO-d6 concentration in water. In all cases, the pump and Stokes power were $I_P = 71\ mW$ and $I_S = 146\ mW$. It can be seen that, at low concentration, the unprocessed CARS signal is dominated by the non-resonant background. However, in panel (c) it can be seen that a background signal also emerges for AM-SRS microscopy. For a discussion, see the text.

As shown in Fig. 2(c), the AM-SRS Raman spectra exhibit nonresonant signals which will limit the sensitivity at low concentrations. As is well known in SRS, this background can be due to three nonlinear effects: resonant two photon absorption (TPA), thermal lens effects averaged over multiple laser pulses (TL) and cross phase modulation (XPM). In order to experimentally determine the origin of the unwanted background shown in Fig. 2(c), we studied a completely non-resonant medium - pure water - which does not exhibit nonlinear absorption at the wavelength used here. Using the same experimental setup, we recorded Raman spectra via AM-SRS in a dilute solution of 0.6 % (88 mM) DMSO-d6 in water (Fig. 3(a)) and in pure water (Fig. 3(b)). It can be seen that the background is present in both cases. As is well known, pure water doesn't exhibit pump-Stokes TPA at the wavelengths used here and, therefore, the broad background signal seen in Fig. 3(b) must be due to either XPM or TL. In the present SRL

#243330 Received 22 Jun 2015; revised 8 Sep 2015; accepted 11 Oct 2015; published 19 Oct 2015

implementation, the SRS signal results in a loss of pump signal power (ΔI_p): an induced lens resulting from TL and/or XPM can modify the divergence of the forward propagating SRS signal. Due to our detection geometry, not all forward propagating light is collected (i.e. vignetting due to the physical size of the photodiode sensor) and, therefore, such induced lens effects can appear as a loss and therefore contribute a background to the SRS hyperspectral scan.

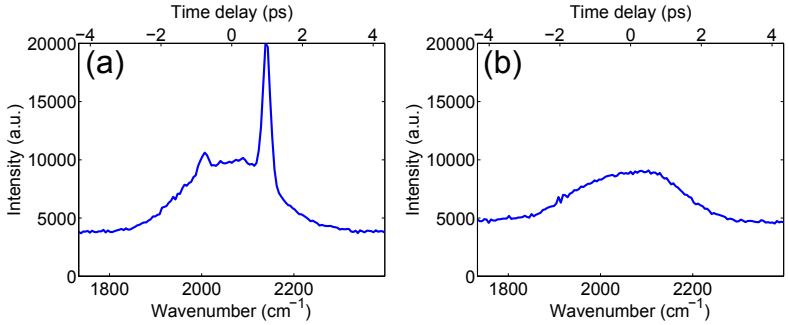

Fig. 3. (a) AM-SRS spectrum of 0,6 % (88 mM) DMSO-d6, showing a nonresonant signal. Here $I_p = 61\ mW$ and $I_S = 95\ mW$. (b) AM-SRS spectrum of pure water also reveals a very similar nonresonant background signal. Here $I_p = 56\ mW$ and $I_S = 151\ mW$. The upper x axis denotes the time delay difference between the pump and the Stokes pulses. With pure water ruling out two-photon absorption, this leaves two possible candidates for the background signal: thermal lensing (TL) and cross-phase modulation (XPM).

Furthermore, from Fig. 3 we can see that the magnitude of the nonresonant signal depends on the time delay between the pump and the Stokes beams (recall that in the chirped pulse scheme, Raman tuning is achieved via scanning the time delay between the linearly chirped pump and Stokes pulses). Since TL is averaged over multiple laser pulses, changing the time delay (by a few picoseconds) between the pump and the Stokes pulses shouldn't change any thermal nonresonant signals because the heating processes due to the modulated (in this implementation) Stokes beam should have a much longer focal-volume averaged dissipation time - on the order of nanoseconds. As seen in Fig. 3, the maximum time delay between the two pulses is in the few picosecond range, orders of magnitude shorter than the heat dissipation time scale. Therefore, the nonresonant signals seen in Fig. 3 cannot be due to TL. This leaves (for the samples under study here) XPM as the remaining possibility. We note that if TL effects were observed, they could be minimized [23, 26, 31, 32] by implementing a polarization modulation (PM) scheme. Indeed, TL is a photothermal effect averaged over many laser pulses and is due to energy from one laser heating the sample (via weak absorption but integrated over many pulses), leading to a temperature and, hence, refractive index gradient which modifies the propagation of the other laser beam. The total heating and, therefore, TL depends on how strongly the sample absorbs the modulated laser beam and on the power in this laser beam. In AM-SRS microscopy, thermal effects are due to the change of power over a single modulation period. Therefore, in order to avoid TL background signals, either (i) amplitude modulation should be avoided or (ii) a collection geometry which integrates the total forward propagating power must be implemented. The former condition can be readily achieved through PM-SRS microscopy where we can ensure the same average power on both polarization axes, resulting in constant average power over the modulation cycles, thereby minimizing thermal lens effects. The complete cancellation of thermal effects in a PM scheme will ultimately depend on the precision with which the optical power can be balanced between the two polarization axes and on the nature of the sample.

The nonresonant background being caused, in the present samples, by XPM, we assume that

#243330 Received 22 Jun 2015; revised 8 Sep 2015; accepted 11 Oct 2015; published 19 Oct 2015

the background signal is coming from the solvent which is, in our case, water. We consider the XPM intensity to be proportional to the refractive index variations experienced by the Stokes beam, which is given by [28]

$$I_{XPM} \propto \delta n_p^a = 3\frac{\chi^{(3)}_{XPM} I_S^a}{n_p n_S \varepsilon_0 c} \tag{1}$$

where the superscript $a = \|, \perp$ represents the orientation of the polarization vector of the Stokes beam with respect to the pump beam (see Fig. 1(d)), I_S^a is the intensity of the Stokes beam along the polarization axis and $\chi^{(3)}_{XPM}$ is the cross phase nonlinear susceptibility, given by (using the convention of Butcher and Cotter) [37]

$$\chi^{(3)}_{XPM} = \chi^{(3)}(-\omega_p, \omega_S, -\omega_S, \omega_p). \tag{2}$$

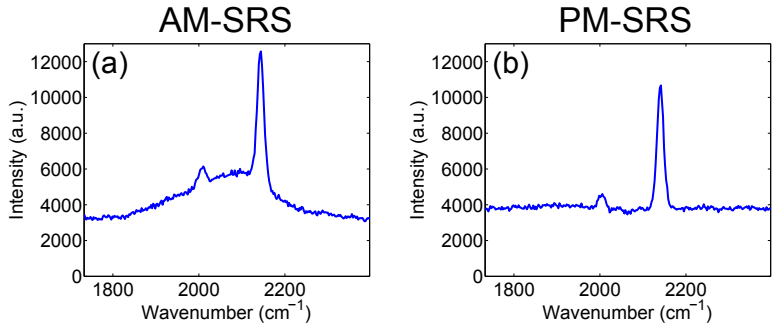

Fig. 4. Spectral scans of 0.6 % (88 mM) DMSO-d6 solution using (a) AM-SRS and (b) PM-SRS. The laser powers were $I_p = 61\ mW$, $I_S^{\|} = 95\ mW$ and $I_S^{\perp} = 174\ mW$. It can be seen that the PM effectively removes the background due to XPM.

The cross phase nonlinear susceptibility terms are elements of a third rank tensor and since, for the solvent, we are far from resonance in the spectral region analysed, we consider $\chi^{(3)}_{XPM}$ to be independent of frequency. In isotropic media such as liquid water, the only nonvanishing elements are $\chi^{(3)}_{1111}$, $\chi^{(3)}_{1122}$, $\chi^{(3)}_{1212}$ and $\chi^{(3)}_{1221}$ [38]. In our detection geometry, only two tensor elements play a role: $\chi^{(3)}_{1111}$, where the polarization vectors of the pump and Stokes beams are both aligned parallel with respect to the same polarization axis; and $\chi^{(3)}_{1221}$ where the polarization vectors of the pump and Stokes beams are aligned orthogonally. For the PM-SRS scheme, the refractive index variation is given by the difference in refractive index between the parallel ($\delta n_p^{\|}$) and perpendicular ($\delta n_p^{\perp}$) polarization alignment. As the XPM signal is proportional to the refractive index variation, the ratio of the AM-SRS and PM-SRS XPM signal is given by:

$$\begin{aligned}\frac{\Delta I_{AM}^{XPM}}{\Delta I_{PM}^{XPM}} &= \frac{\delta n_p^{\|}}{\delta n_p^{\|} - \delta n_p^{\perp}} \\ &= \frac{\chi^{(3)}_{1111} I_S^{\|}}{\chi^{(3)}_{1111} I_S^{\|} - \chi^{(3)}_{1221} I_S^{\perp}} \\ &= \frac{I_S^{\|}}{I_S^{\|} - \rho I_S^{\perp}}\end{aligned} \tag{3}$$

#243330 Received 22 Jun 2015; revised 8 Sep 2015; accepted 11 Oct 2015; published 19 Oct 2015

where $\rho = (\chi^{(3)}_{1221})/(\chi^{(3)}_{1111})$ is the depolarization ratio of the solvent. The depolarization ratio measures the degree of depolarization of the scattered field with respect to the incident field. It ranges from 0 to 0.75: for high symmetry parallel polarized bands $\rho \approx 0$, whereas for a fully depolarized band $\rho = 0.75$ [39]. The depolarization ratio for liquid water varies across the Raman spectrum: in the region of interest here, from 1750 cm^{-1} to 2400 cm^{-1}, it achieves an average value of 0.6 [40]. In contrast, for DMSO-d6, ρ assumes a value close to 0 for the Raman bands at 2000 and 2125 cm^{-1} [41]. It is worth noting that a depolarized DMSO-d6 Raman band exists at ~ 2250 cm^{-1} with a depolarization ratio of 0.75. This band, however, is too far from the center of our set spectral range to be resolved at low concentration. The PM-SRS scheme described here would have poor contrast for this particular Raman band.

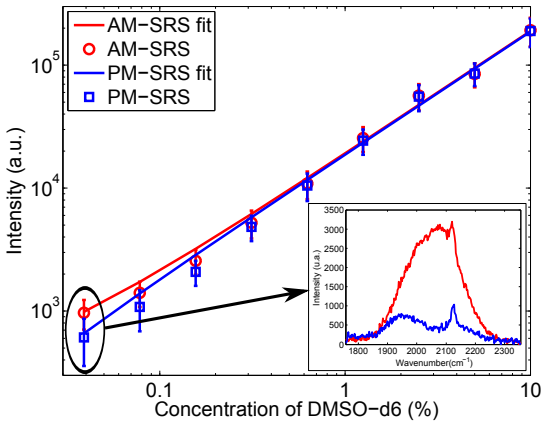

Fig. 5. Log-log plots of AM- and PM-SRS signals as a function of the DMSO-d6 concentrations, ranging between 0.039 % (5.5 mM) and 10 % (1.4 M). The laser powers were the same for both the AM and PM SRS measurements: $I_p = 64$ mW, $I_S^{\parallel} = 106$ mW and $I_S^{\perp} = 178$ mW. In the inset, we show the raw SRS spectra at the lowest DMSO-d6 concentration recorded, 0.039 % (5.5 mM).

The terms on the left side of Eq. (3) represent the ratio of the XPM signals when using PM-SRS and AM-SRS. Therefore, it suffices to measure the magnitude of the background signals for $I_S^{\parallel} = I_S^{\perp}$ in order to obtain the depolarization value of the sample component causing the XPM signal; liquid water in our case. Using this approach, we were able to identify the origin of the background signals shown in Fig. 3. We measured the depolarization ratio of pure water by recording the associated Raman spectra, using AM-SRS and PM-SRS, by setting the laser power to be the same for both polarizations of the Stokes beam (Fig. 1 with $I_S^{\parallel} = I_S^{\perp} = 152\,mW$). We determined a depolarization ratio ρ of 0.59 for liquid water which is in good agreement with values found in the literature [40]. This means that the background signal seen in Fig. 3 is due to XPM and, therefore, it can be minimized via our PM scheme. The PM-SRS yields a differential measurement between the SRS signals produced in the parallel and perpendicular geometries. This differential is controlled by varying the power between the two polarization axes of the Stokes beams ($I_S^{\parallel}$ and $I_S^{\perp}$ in Eq. (3)). Indeed, as shown in Fig. 4, we were able to largely remove XPM effects using the PM-SRS modulation scheme. From Eq. (3), one would expect to use $\frac{5}{3}$ more power in one arm ($I_S^{\perp}$) than in the other ($I_S^{\parallel}$) in order to completely cancel the XPM term. For the data shown in Fig. 4, we used $I_S^{\parallel} = 95$ mW and $I_S^{\perp} = 174$ mW, a 10 % larger ratio. This discrepancy is likely caused by some of the optical elements in the microscope setup of Fig. 1

#243330 Received 22 Jun 2015; revised 8 Sep 2015; accepted 11 Oct 2015; published 19 Oct 2015

being polarization dependent, inducing more loss on one polarization axis. For this reason, in order to balance the XPM signals, we had to compensate with about 10 % more power input. It is worth noting that our PM-SRS method is best suited to highly polarized Raman bands. For the PM scheme, the attenuation of the signal is directly proportional to the depolarization ratio: a Raman band having a large depolarization ratio will be strongly attenuated. In cases where the depolarization ratio of the probed Raman band is equal to or greater than the depolarization ratio of the XPM signal, the SRS signal could vanish or obtain a negative value. In such cases, the AM modality of our combined approach then applies. Our implementation easily converts from PM- to AM-SRS simply by blocking (or chopping) one arm of the PM scheme output. For a known sample, the relevant depolarization ratios can be obtained from the literature or measured directly by comparing the intensity difference between the AM and PM signals. We further note that the presence of net birefringence will reduce the contrast in our PM scheme, For example, in the most extreme case that the modulated beam achieve circular polarization in the medium, the PM-SRS contrast will in fact vanish. In the more realistic case of slight elliptical polarization of the modulated beam, the PM-SRS modulated depth will be reduced and therefore the imaging contrast will decrease (the "background" due to imperfect cancellation of XPM and TL will begin to appear as it does in the AM case). Nevertheless, the flexibility of our AM-PM approach allows us to optimize to the extent possible - but only on average across the ROI - the SRS contrast for a given sample.

In order to characterize our PM-SRS method, we carried out a series of measurements on dilute solutions of DMSO-d6 in water, ranging from 10 % (1.4 M) to 0.039 % (5.5 mM). We also directly compared the sensitivity limits, in term of spectral peak visibility, of the two modulation schemes, as shown in Fig. 5. These results show that we are able to unambiguously detect, via its Raman spectrum, DMSO-d6 at a low concentration of 0.039 % (5.5 mM). In our current implementation it seems that, at the low concentration limit, the two modulation scheme seem to differ little in term of intensity contrast. This is due to the fact the spectral signal-to-noise ratios are close to one at the lowest concentrations, meaning that the system electronic noise is still playing an important role at the smallest signal levels for each measurement. We expect, therefore, that improvements in electronic signal recovery will push AM/PM-SRS sensitivity limits even further. We discuss, below, the improved Raman peak contrast (and therefore chemical contrast) offered by the PM-SRS scheme for samples in which XPM is the dominant background.

In order to demonstrate the advantages of PM for hyperspectral imaging, we performed both AM-SRS and PM-SRS imaging of an artificial sample composed of low concentration (0.3 %, 44 mM) DMSO-d6 droplets in octadecene. The only Raman resonances in the spectral region 1750 cm^{-1} to 2400 cm^{-1} are due to DMSO-d6: octadecene has no Raman resonances in this range. The results are shown in Fig. 6. It can be seen that Raman spectral identification (i.e. Raman peak visibility) of the target molecule DMSO-d6, via its main resonance at 2150 cm^{-1}, is significantly improved in such samples by the PM modulation scheme.

4. Conclusion

Implementations of SRS microscopy based on spectral focusing can be easily integrated with other nonlinear optical imaging modalities such as SHG and TPEF, providing a simple yet powerful approach to label-free hyperspectral multi-modal imaging. In this paper, we presented a new modulation scheme for spectral focusing SRS microscopy based on polarization modulation (PM-SRS). Our PM-SRS scheme was able to largely remove background signals due to XPM by appropriately balancing the power in the two (parallel and perpendicular) Stokes beams. Depending on the origin of the background signals, which in turn will vary with the specific sample under analysis, we are able to remove XPM effects and potentially TL with

#243330 Received 22 Jun 2015; revised 8 Sep 2015; accepted 11 Oct 2015; published 19 Oct 2015

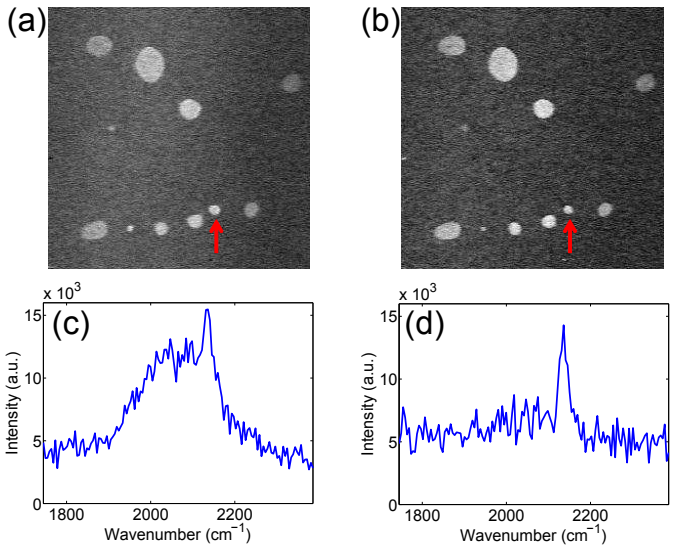

Fig. 6. Hyperspectral SRS imaging at low concentration. (a) AM-SRS and (b) PM-SRS hyperspectral images of 0.3 % (44 mM) DMSO-d6 droplets in an octadecene medium. The spectra associated with the droplet shown by the arrow are given in panel (c) for AM-SRS and (d) for PM-SRS. In both schemes, $I_p = 57\ mW$, $I_S^{\parallel} = 110\ mW$ and $I_S^{\perp} = 176\ mW$. It can be seen that, although the image intensity contrast appears similar in both AM and PM schemes, the spectral identification (Raman peak visibility) of the target molecule is much clearer in the PM scheme. The images size are $270 \times 270\ \mu m$.

our scheme. In order to compensate for XPM effects, the power should be adjusted in the two polarization axes as dictated by the depolarization ratio. Our scheme also readily permits both AM- and PM-SRS microscopy. We compared the detection limits for AM-SRS and PM-SRS microscopy and showed the expected linear relation between SRS signal and concentration. We also compared AM-SRS with PM-SRS in a hyperspectral imaging modality. We showed that PM-SRS enhances the spectral visibility of the vibrational Raman bands at low concentrations. The high sensitivity provided by PM-SRS, coupled with its enhanced "chemical" (i.e. Raman band visibility) contrast, should allow for hyperspectral SRS microscopy in a range of samples. We caution, however, that for samples with significant birefringence or for Raman modes with a large depolarization ratio, the PM-SRS modality will have reduced contrast. In such case, the AM-SRS scheme afforded by our implementation will still apply. Furthermore, when the samples birefringence or XPM background vary spatially across a region of interest (ROI), the balancing of the arms in PM-SRS can only be achieved only on average across the ROI. Nevertheless, our implementation permits considerably flexibility in varying amplitude and polarization, as well as lock-in frequency and phase and, therefore, we anticipate that this approach will find use in optimizing Raman-based image contrast in a range of samples. Finally, we note that, although in the present scheme we were limited to SRL detection, the PM-SRS approach should perform even more favorably in a Stimulated Raman Gain (SRG) scheme. This is because absorptive signals due to two-photon absorption are always a loss whereas SRG is always a gain - and is therefore "out of phase" in a lock-in amplifier detection scheme [42] - meaning that both TL and XPM effects should be largely removed by a PM-SRG scheme. We are currently developing this approach, which will be discussed in a future publication.

#243330 Received 22 Jun 2015; revised 8 Sep 2015; accepted 11 Oct 2015; published 19 Oct 2015

Acknowledgments

The authors acknowledge the financial support of the Natural Sciences and Engineering Research Council of Canada (NSERC). We are grateful to R. Lausten (NRC), E. Potma (UC Irvine) and J-X Cheng (Purdue) for helpful technical advice. AS acknowledges the support of the Canadian Research Chairs.

#243330 Received 22 Jun 2015; revised 8 Sep 2015; accepted 11 Oct 2015; published 19 Oct 2015